A falsifiable Higher–Dimensional Blast imprint in the nanohertz stochastic gravitational–wave background

Ricardo Maldonado. DOI: 10.5281/zenodo.17968738.

December 16, 2025

Abstract

We present a blast-only, observationally falsifiable hypothesis: a short, violent episode in an early higher-dimensional phase sets initial conditions for our observable Universe and leaves a surviving low-energy imprint as a cosmological stochastic gravitational-wave background (SGWB). We represent the imprint with a smooth broken power-law (SBPL) energy-density spectrum with a knee in the pulsar timing array (PTA) band, and we evaluate the model using a transparent set of "guardrail" tests. For a canonical parameter point, we find consistency with the radiation-budget constraint (physical $\Delta N_{\rm eff}$), strong multi-band safety relative to LISA/LVK frequency ranges, cross-PTA knee coherence, and (example) GR ringdown consistency. In a PTA-band screening comparison using binned free-spectrum points (Gaussian approximation), SBPL curvature is preferred over the canonical supermassive black-hole binary (SMBHB) power law and over a generic single power law with a free slope. We also test a two-component mixture (SBPL+SMBHB) and find it is not favored by BIC relative to SBPL alone on the bundled screening dataset. We additionally report a transparent marginal-likelihood (evidence) screening calculation under stated priors.

1 Phenomenological SGWB model

We use an SBPL template for the present-day SGWB energy density,

$$\Omega_{\rm gw}(f) = \Omega_k \left[\frac{(f/f_k)^{\alpha_1\Delta} + (f/f_k)^{\alpha_2\Delta}}{2}\right]^{-1/\Delta}. \tag{1}$$

The knee f_k marks the transition. For $\alpha_1 > 0$ and $\alpha_2 < 0$, the asymptotic behavior is $\Omega \propto f^{-\alpha_2}$ for $f \ll f_k$ and $\Omega \propto f^{-\alpha_1}$ for $f \gg f_k$.

1.1 Two analytic shape diagnostics

Two closed-form "shape invariants" are useful when comparing to PTA spectra:

- **Peak location.** For $\alpha_1 > 0 > \alpha_2$, the SBPL has a single maximum at

$$\frac{f_{\rm peak}}{f_k} = \left(\frac{-\alpha_2}{\alpha_1}\right)^{1/[\Delta(\alpha_1-\alpha_2)]}. \tag{2}$$

  For the canonical $(3, -2, 2)$ this gives $f_{\rm peak} \simeq 0.96\, f_k$.

- **Knee slope.** The logarithmic slope at the knee is

$$\left.\frac{d\ln\Omega}{d\ln f}\right|_{f_k} = -\frac{\alpha_1+\alpha_2}{2}. \tag{3}$$

- **Knee curvature.** A single power law has zero curvature in $\ln\Omega$ vs $\ln f$, whereas SBPL has

$$-\left.\frac{d^2\ln\Omega}{d(\ln f)^2}\right|_{f_k} = \frac{(\alpha_1-\alpha_2)^2\,\Delta}{4}. \tag{4}$$

  Measuring nonzero curvature in a PTA-inferred free spectrum is therefore a direct discriminator.

1.2 Canonical point used here

Parameter	Value
Ω_k	8.00×10^{-9}
f_k [Hz]	3.16×10^{-8}
α_1	3.0
α_2	-2.0
Δ	2.0

2 Candidate higher-dimensional embedding (optional)

Equation (**??**) is used here as a *phenomenological* template. One concrete higher-dimensional interpretation is a brane–world transition in which the early expansion history differs from standard 4D radiation domination.

As an example, in Randall–Sundrum–type brane cosmology the effective 4D Friedmann equation can receive a high-energy correction and a Weyl ("dark radiation") term,

$$H^2 = \frac{8\pi G}{3}\,\rho\left(1+\frac{\rho}{2\lambda}\right)+\frac{\Lambda_4}{3}+\frac{\mathcal{C}}{a^4}, \tag{5}$$

where λ is the brane tension and $\mathcal{C}$ parameterizes the projected 5D Weyl contribution. A short "blast" in the bulk/brane system can excite tensor modes; modes that re-enter the horizon during the ρ^2-dominated regime ($\rho \gg \lambda$) evolve with a different transfer function than modes re-entering after the transition $\rho\sim\lambda$, producing an effective spectral knee.

A useful calibration is the transition temperature

$$T_\times = \left[\frac{60\,\lambda}{\pi^2\,g_*(T_\times)}\right]^{1/4}, \tag{6}$$

and the present-day frequency corresponding to a mode with $k_* \equiv \xi\,a_* H_*$ is approximately

$$f_\times \simeq 2.6\times10^{-8}\,\mathrm{Hz}\left(\frac{T_\times}{\mathrm{GeV}}\right)\left(\frac{g_*}{100}\right)^{1/6}\xi. \tag{7}$$

Finally, the Weyl (dark-radiation) term can be expressed as an effective $\Delta N_{\rm eff}$ via

$$\frac{\Omega_{\rm dr}}{\Omega_\gamma} = \frac{7}{8}\left(\frac{4}{11}\right)^{4/3}\Delta N_{\rm eff}. \tag{8}$$

In such embeddings, $(f_k, \Delta N_{\rm eff})$ can be viewed as two observables constraining higher-dimensional parameters $(\lambda, \mathcal{C})$. We emphasize that the present work does *not* assume this specific microphysics; it is included only to show how a measured knee can map onto higher-dimensional physics.

3 Guardrail tests (falsifiable gates)

We emphasize: passing a gate means the parameter point is *not ruled out* by that test; it is not a confirmation of an origin mechanism.

3.1 Radiation budget: physical $\Delta N_{\rm eff}$

We compute

$$\Omega_{\rm gw,tot} = \int_{f_{\rm min}}^{f_{\rm max}} \Omega_{\rm gw}(f)\, d\ln f, \qquad \Delta N_{\rm eff} = \frac{8}{7}\left(\frac{11}{4}\right)^{4/3} \frac{\Omega_{\rm gw,tot}}{\Omega_\gamma}. \tag{9}$$

For the canonical point, $\Delta N_{\rm eff} = 7.09 \times 10^{-4}$. For fixed SBPL shape, $\Delta N_{\rm eff}$ scales linearly with Ω_k. A useful closed form for the integral in Eq. (**??**) (for $\alpha_1 > 0 > \alpha_2$) is

$$\int_0^\infty \Omega_{\rm gw}(f)\, d\ln f = \Omega_k\, I_{\rm SBPL}, \qquad I_{\rm SBPL} = \frac{2^{1/\Delta}}{\Delta(\alpha_1 - \alpha_2)}\, B\!\left(\frac{-\alpha_2}{\Delta(\alpha_1-\alpha_2)}, \frac{\alpha_1}{\Delta(\alpha_1-\alpha_2)}\right), \tag{10}$$

where B is the Euler beta function. For the canonical $(\alpha_1, \alpha_2, \Delta) = (3, -2, 2)$ one finds $I_{\rm SBPL} \approx 1.096$, so $\Omega_{\rm gw,tot} \approx 1.096\,\Omega_k$ and $\Delta N_{\rm eff}$ is strictly linear in Ω_k for fixed shape.

3.2 PTA curvature diagnostic (model-agnostic)

Independently of any specific physical template, a single power law is linear in $\log\Omega$ vs. $\log f$ (zero curvature). We fit the binned PTA free-spectrum points with (i) a linear model in $\log_{10} f$ and (ii) a quadratic model. On the bundled dataset, the quadratic term is detected at $|c|/\sigma_c \simeq 3.22\sigma$ and the curved model is favored by ΔBIC(linear − quadratic) $\simeq 8.08$ (Fig. **??**). This provides a model-agnostic test for a knee/turnover in the PTA band.

3.3 PTA spectral-shape screening comparison (ΔBIC)

Using binned PTA free-spectrum points with Gaussian errors, we compare SBPL curvature to: (i) an SMBHB power law (fixed $\Omega \propto f^{2/3}$), (ii) a generic single power law with a free slope, (iii) a flat Ω proxy (cosmic-string-like plateau). On the bundled example free-spectrum, SBPL is preferred over SMBHB by ΔBIC $\simeq 26.2$, corresponding to $\log_{10}$ BF $\simeq 5.69$ under the usual BIC-to-Bayes-factor approximation.

We additionally fit a two-component mixture $\Omega = \Omega_{\rm SBPL} + \Omega_{\rm SMBHB}$ (two amplitudes, fixed shapes). The im

3.4 Prior sensitivity of evidence screening (screening)

Bayes factors depend on priors. We therefore repeat the binned-Gaussian evidence calculation for several prior widths in $(\log_{10}\Omega_k, \log_{10} f_k)$ (SBPL) and in $\log_{10} A$ (SMBHB). Across broad-to-moderate prior choices, we find $\log_{10}$ BF $\simeq$ 3.6–4.2 in favor of SBPL over SMBHB, indicating qualitative robustness. Extremely tight priors can inflate Bayes factors via prior-volume effects, so this step is a robustness check rather than a substitute for a full PTA timing-residual likelihood analysis.

provement in χ^2 is small and the Occam penalty dominates: ΔBIC(mix − SBPL) ≈ 2.06, so the mixture is *disfavored* relative to SBPL alone (screening dataset).

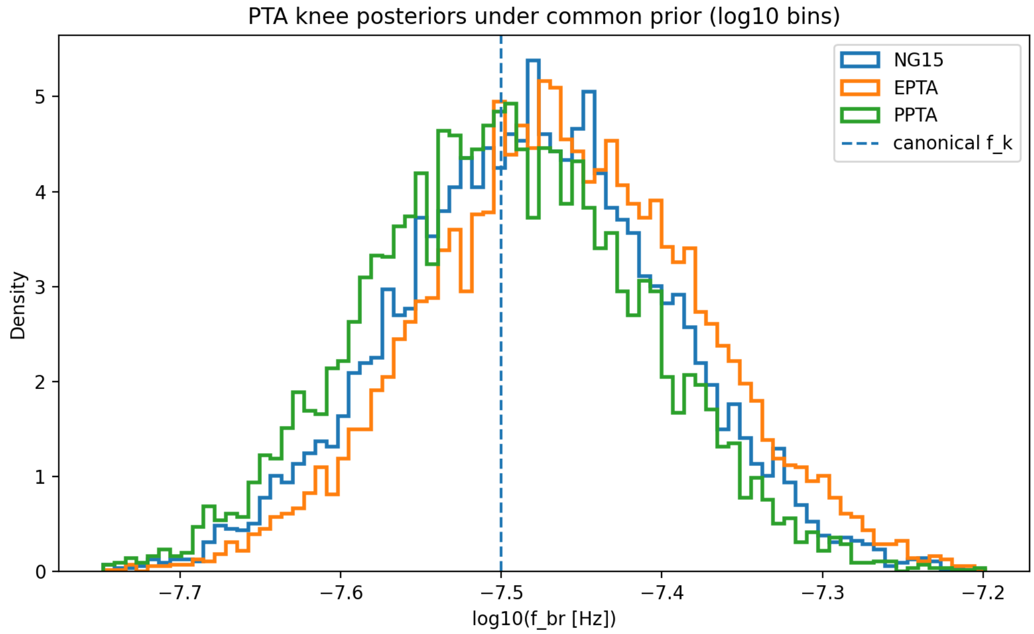

Figure 1: Knee-frequency posteriors from independent PTAs under a common prior (histograms in $\log_{10} f_{\mathrm{br}}$).

3.5 PTA-band evidence screening (marginal likelihood)

As an additional screening step (still not a full PTA timing-residual likelihood), we compute a marginal likelihood under stated priors. On the bundled example dataset, the evidence calculation yields $\log_{10} \mathrm{BF} \approx 3.95$ (SBPL with scanned knee) or ≈ 5.40 (SBPL with fixed canonical knee) relative to SMBHB.

3.6 Cross-PTA knee coherence (PCI)

PCI summarizes agreement of independent PTA knee-frequency posteriors under a shared prior via histogram intersections in $\log_{10} f_k$. On bundled example knee posteriors, PCI ≈ 0.87 (pass threshold 0.80).

3.7 Late-time GR null (ringdown ϵ; example workflow)

A pooled example ringdown workflow yields $\epsilon = 0.0015$ with a 68% interval $[-0.0096, 0.0127]$, consistent with the GR null $\epsilon = 0$.

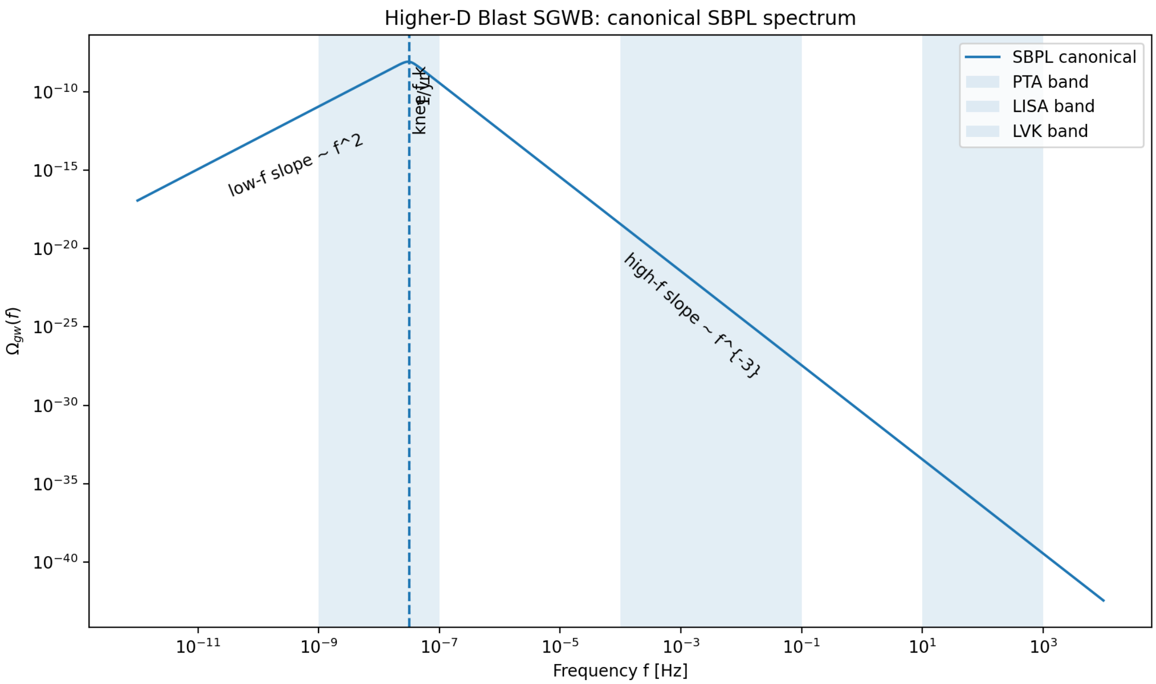

Figure 2: Canonical SBPL spectrum across PTA/LISA/LVK frequencies.

3.8 Gate summary table (canonical)

Test	Quantity	Canonical result (screening inputs)
Radiation budget	$\Delta N_{\rm eff}$	7.09×10^{-4}
Multi-band checkpoints	$\Omega_{\rm gw}(3\,\mathrm{mHz})$	1.32×10^{-23}
	$\Omega_{\rm gw}(25\,\mathrm{Hz})$	2.28×10^{-35}
PTA coherence	PCI (median)	0.866
PTA model choice (screening)	ΔBIC(SMBHB$-$SBPL)	26.21
	$\log_{10}$ BF (approx)	5.69
PTA curvature (screening)	$\lvert c\rvert/\sigma_c$; ΔBIC(lin$-$quad)	3.22σ ; 8.08
Ringdown GR null (example)	ϵ pooled (68% CI)	$[-0.0096, 0.0127]$

4 Multi-band predictions

For the canonical SBPL point, the spectrum is extremely suppressed in the LISA and ground-based bands (see Table above), implying that a strong detection by LISA or LVK would falsify the canonical high-frequency tail unless the parameters are modified.

5 Knee-to-epoch mapping (order of magnitude)

If the knee traces a causal scale $k_* = \xi a_* H_*$ during radiation domination, then the observed f_k maps to an epoch temperature T_* and a horizon mass scale. The mapping depends on the dimensionless factor ξ (model-dependent). For reference, the blast-only kit reports representative values:

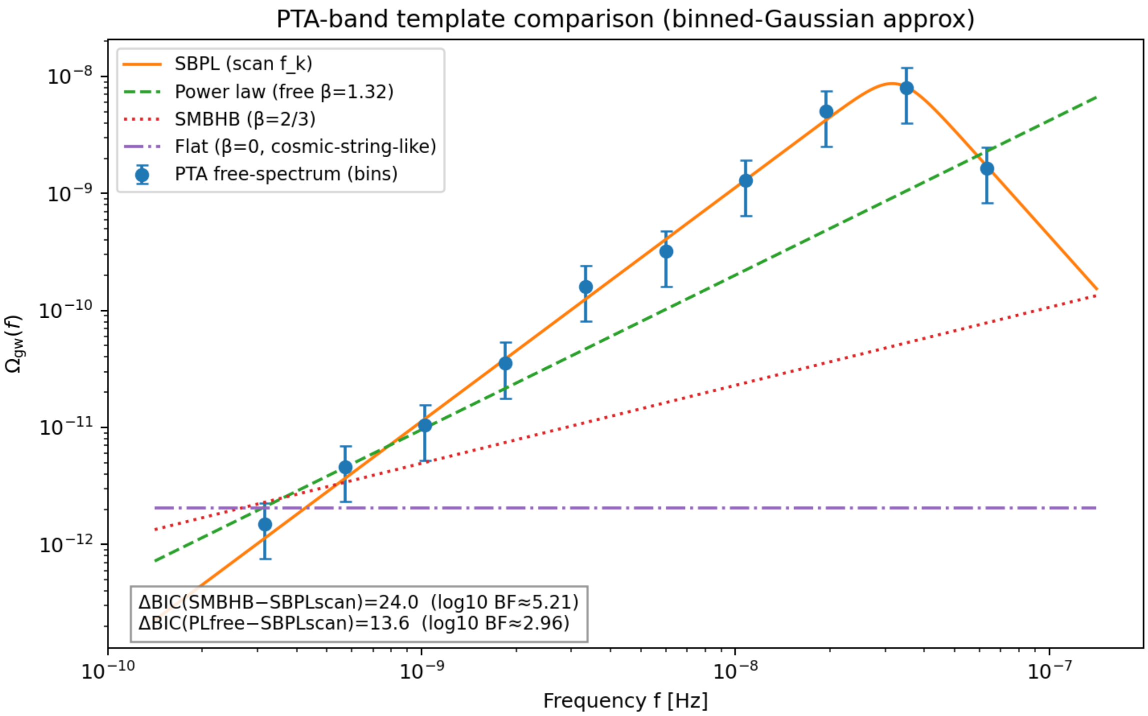

Figure 3: PTA-band template comparison (binned-Gaussian approximation). SBPL curvature is preferred over SMBHB and over a generic single power law with a free slope (example inputs).

- $\xi = 1$: $T_* \approx 1.31\,\mathrm{GeV}$, $t_* \approx 1.8 \times 10^{-7}\,\mathrm{s}$, horizon mass $\approx 0.027\,M_\odot$.
- $\xi = 6.5$: $T_* \approx 0.20\,\mathrm{GeV}$, $t_* \approx 7.6 \times 10^{-6}\,\mathrm{s}$, horizon mass $\approx 1.15\,M_\odot$.

6 Falsifiability roadmap

Key near-term falsifiers include: (i) PTA posteriors converging to an unbroken power law (no knee/curvature); (ii) incompatible knee locations across PTAs under a common prior (low PCI); (iii) PTA-inferred amplitudes that drive ΔN_{eff} above bounds; or (iv) a clear LISA/LVK detection inconsistent with the canonical high-frequency tail.

7 Reproducibility

All scripts, templates, and example inputs used to generate this document's numbers are included in the accompanying referee kit.

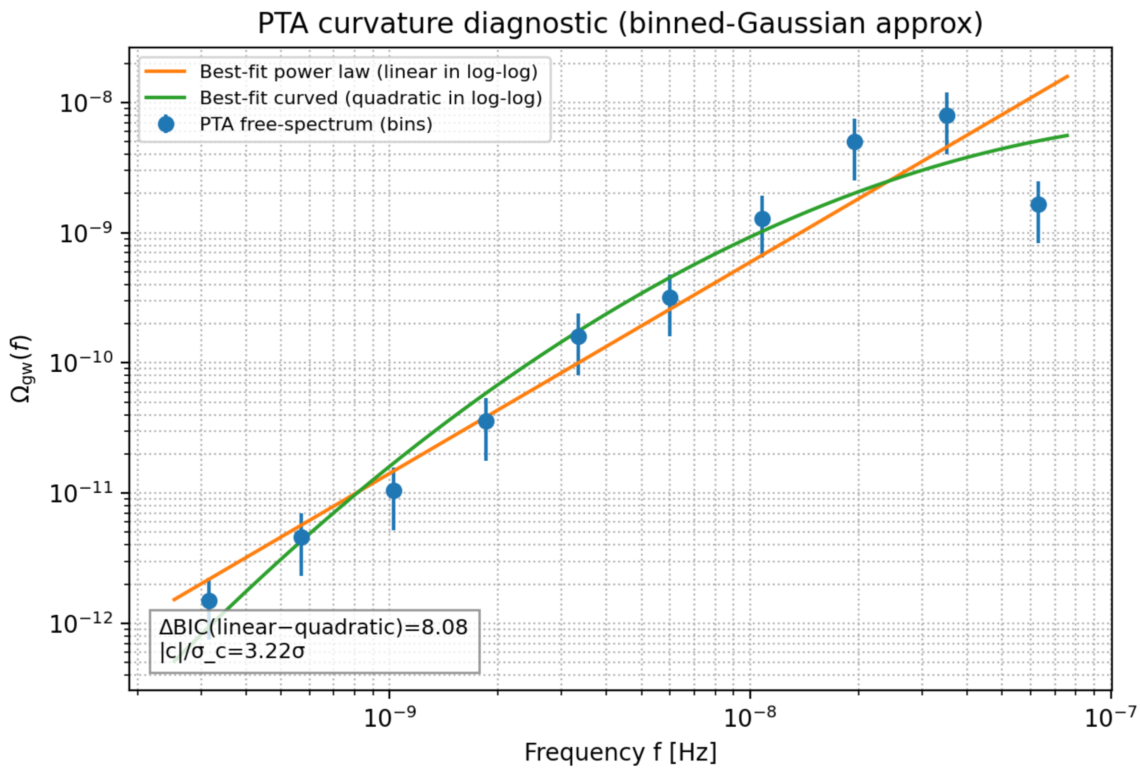

Figure 4: Model-agnostic PTA curvature diagnostic: quadratic vs linear fit in log-log space (binned-Gaussian screening).

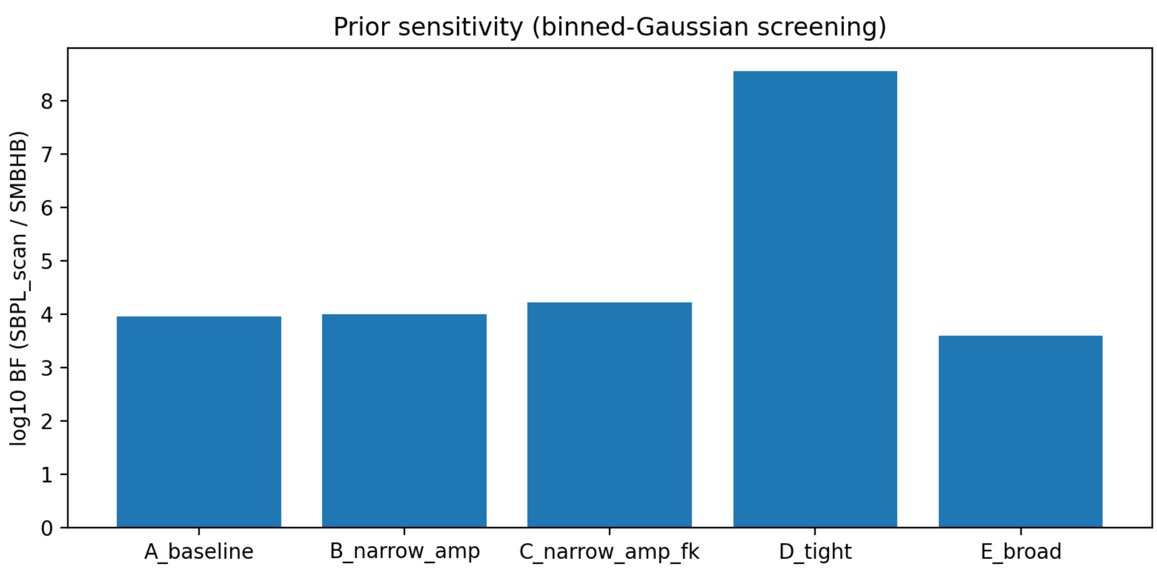

Figure 5: Prior sensitivity of the SBPL-vs-SMBHB evidence screening (binned-Gaussian approximation).

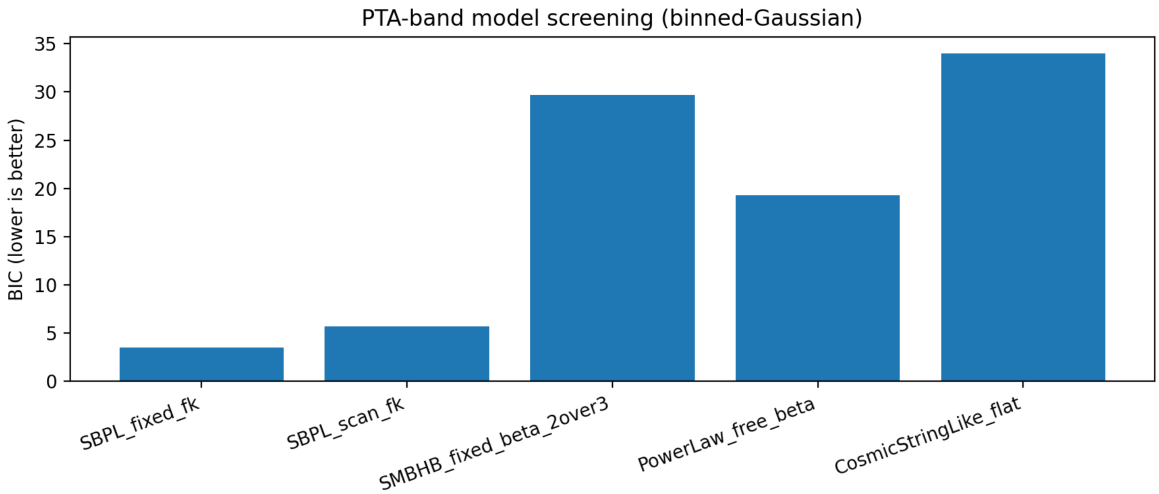

Figure 6: BIC comparison for PTA-band screening templates (binned-Gaussian). Lower is better.

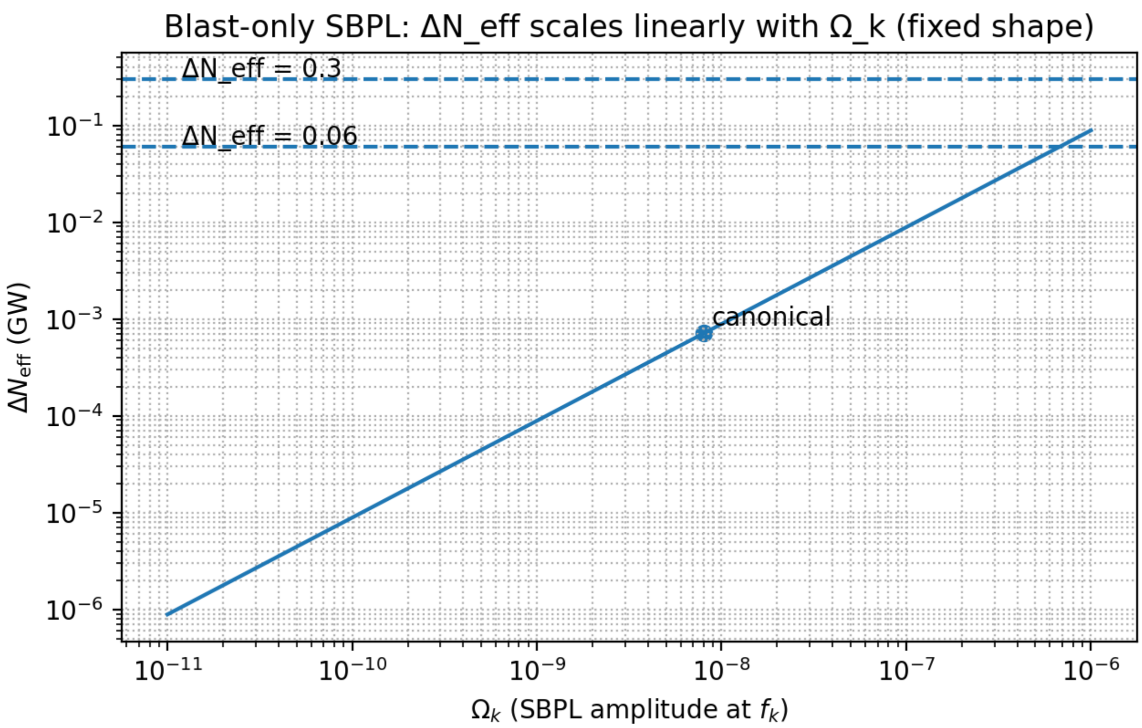

Figure 7: ΔN_{eff} scaling with Ω_k for fixed canonical SBPL shape.

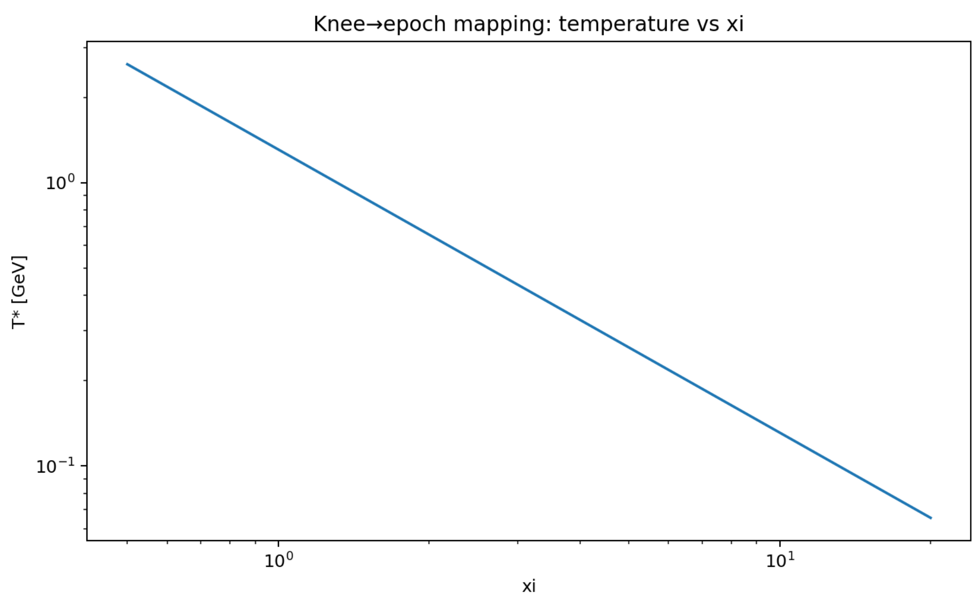

Figure 8: Order-of-magnitude knee-to-epoch diagnostic plot (kit plot).